YTUP

Journal of Thermal Engineering
https://jten.yildiz.edu.tr/
https://doi.org/10.47481/jten.0026

RESEARCH ARTICLE

Computational analysis of blade tip-to-tower clearance effects on horizontal-axis tidal current turbine performance

Zia Ur Rehman[1], Saeed Badshah[2], Majid Baseer[3,*], Mujahid Badshah[4], Moddasir Khan[5], Riaz Hussain[6], Roohullah Khan[7]

[1]Department of Mechanical Engineering, International Islamic University Islamabad, 44300, Pakistan
[2]Department of Mechanical Engineering, International Islamic University Islamabad, 44300, Pakistan
[3]CETHIL UMR 5008, CNRS, INSA Lyon, Université Claude Bernard Lyon 1, Université de Lyon, F-69621, Villeurbanne, France
[4]Department of Mechanical Engineering, International Islamic University Islamabad, 44300, Pakistan
[5]Department of Mechanical Engineering, International Islamic University Islamabad, 44300, Pakistan
[6]Department of Mechanical Engineering, Sarhad University of Science & Information Technology Peshawar, 25000, Pakistan
[7]Department of Mechanical Engineering, International Islamic University Islamabad, 44300, Pakistan

Abstract

Early tidal turbine deployment is expected to occur in relatively shallow waters, where monopile support structures are widely adopted due to their structural simplicity, cost-effectiveness, and ease of installation. However, the influence of tip-to-tower clearance and symmetry boundary conditions on turbine performance and structural loading remains insufficiently understood. This study presents a combined analysis of the effects of tip-to-tower clearance and symmetry boundary conditions on the performance of a horizontal-axis tidal-current turbine (HATCT), using high-fidelity, transient computational fluid dynamics (CFD) simulations. Simulations were performed in ANSYS CFX by solving the Reynolds-Averaged Navier-Stokes (RANS) equations using the Shear Stress Transport (SST) turbulence model and a transient rotor–stator interface. Turbine performance is evaluated using two key coefficients: the coefficient of performance (C_p) and the coefficient of thrust (C_t). A tower diameter of 2 m was considered, with blade tip-to-tower clearances of 7 m, 5 m, 3 m, and 2 m. The corresponding mean cycle C_p values are 0.468, 0.476, 0.470, and 0.472, respectively, while C_t values remain largely unaffected, ranging between 0.86 and 0.87. Although average power shows minimal variation, power output fluctuates notably (approximately 3–4%) as clearance decreases. Additionally, substantial unsteady forces are generated on the tower, which may contribute to increased fatigue loading. The use of symmetry boundary conditions shows negligible impact on prediction accuracy while significantly reducing computational cost. These findings demonstrate that, when structural elasticity effects are accounted for, a blade tip-to-tower clearance approximately equal to the tower diameter is optimal for HATCT systems, providing practical design guidance for tidal turbine support structures.

Keywords: Horizontal axis tidal current turbine, monopile support tower, computational fluid dynamics, blade tower interaction

Cite this article as: Rehman, Z. U., Badshah, S., Baseer, M., Badshah, M., Khan, M., Hussain, R., & Khan, R. (2026). Computational analysis of blade tip-to-tower clearance effects on horizontal-axis tidal current turbine performance. Journal of Thermal Engineering, 12(4), 1233–1242. https://doi.org/10.47481/jten.0026

1. Introduction

Nearly one degree of global warming has been observed and is primarily attributed to anthropogenic activity since the pre-industrial era, according to the Intergovernmental Panel on Climate Change (IPCC). Global warming is associated with the emission of greenhouse gas emissions ($C0_2$, CH4, and N_2O), which result from the excessive reliance on fossil fuels [1-4]. In response, the Paris Agreement sets a goal of limiting global warming to 2°C above pre-industrial levels this century. Achieving this target necessitates a global transition from-conventional fossil fuel-based energy systems to sustainable, renewable energy alternatives.

There are numerous renewable energy resources, including biomass, wind energy, photovoltaic solar energy, solar thermal

*Corresponding Author
E-mail Adress: majid.baseer@insa-lyon.edu.fr

Submitted: 11 March 2025 ; **Accepted:** 26 June 2025

This paper was recommended for publication in revised form by Editor-in-Chief Ahmet Selim Dalkılıç

electricity, low-temperature solar thermal energy, hydroelectricity, geothermal energy and marine energy [5-8]. Tidal energy is one of the renewable resources that has the greatest potential because it is very predictable and its energy density is relatively high [9]. The flows associated with tides, which are generated by lunar gravitational forces acting on the Earth's surface, occur in a cyclic, predictable manner that can be used for the generation of renewable energy [10].

Horizontal-Axis and Vertical-Axis Tidal Current Turbines (HATCT and VATCT), oscillating hydrofoils, tidal kites, ducted turbines and tidal range systems are all examples of various energy extracting devices based on tidal currents [11, 12]. The HATCT design is the most developed design among others and approximately 76% of research activity regarding energy extraction from tidal currents is related to this design [13]. Therefore, the first generation of tidal energy systems appears to converge toward the HATCT design [14].

Several authors have observed that marine flows may significantly affect the performance of HATCT (including near- and far-wake characteristics). In particular, velocity shear conditions may have a considerable effect on turbine performance [15]. Apart from velocity shear, the effects of the wave-current interaction, bathymetry, free surface proximity and boundaries effects have been broadly investigated [16]. For example, it has been observed that the presence of wave enhances turbine performance, whereas blockage ratio effects were marginal at low TSR values but increase at higher TSR values [10, 17].

The hydrodynamic and structural performance of a turbine is heavily influenced not only by environmental flow conditions but also by the geometric configuration of turbine components. The main components of a tidal turbine are the rotor, the nacelle, and the support structure. Several authors have shown that the design of the nacelle has an insignificant effect on turbine performance [18], but the design of the support structure-in particular, the tower-can be a significant factor.

The monopile tower, a widely accepted support concept across configurations, has attracted interest for first-generation tidal devices, particularly for shallow-water installations. This support has been extensively used in the wind energy sector, but its design criteria need to be re-evaluated for tidal applications due to vast differences between air and water flow conditions.

Although various features of monopile-supported tidal turbines have been explored, further analysis is still needed to understand the overall impact of transferring wind turbine support structures into a marine environment. One significant effect on the turbine that can be attributed to the support structure is the 'tower shadow effect'; the presence of the support structure locally alters the incoming flow at the rotor, and may therefore affect turbine power output [19]. The effects depend on various parameters, such as tower shape, and size, the distance between the blade tip and the tower, and structural flexibility. Generally, there appears to be some consensus that cylindrical tower sections are likely to have less impact on turbine performance than alternative cross-sectional shapes, such as square or oval [20]. and studies have found that elasticity in the tower can be related to the variability of the turbine power output [14].

Previous work analyzed the effect of tower diameter on turbine performances [21]. Accordingly, the present work analyzes the effect of blade tip-to-tower clearance on the hydrodynamic performance of HATCTs.

This paper is organized into five sections. Section 1 presents the background and motivation for the study. Section 2 describes the methodology and materials, with Sections 2.1 and 2.2 giving details about the computational domain and meshing approach, respectively. Section 3 defines the performance parameters. Section 4 discusses the simulation results. Finally, Section 5 provides a summary of the key findings and conclusions.

2. Materials & methods

The full-scale St. Anthony Falls Laboratory (SAFL) Reference Model 1 (RM1) turbine, featuring a twenty-meter diameter rotor and blades shaped based on the NACA 4415 profile [22], is simulated using transient analysis for ten rotations. The simulation is conducted using a transient rotor-stator approach while varying the tip-to-tower clearance in the CFX package of ANSYS. CFX is a node-centered finite volume solver [23].Within a set of control volumes, the continuity and momentum equations given below as Equations (1) and (2) respectively are solved in ANSYS CFX [24].

$$\frac{\partial \rho}{\partial t} + \nabla \cdot [\rho V] = 0 \quad (1)$$

$$\frac{\partial (\rho U)}{\partial t} + \nabla \cdot (\rho U * U) = -\nabla p + \nabla \cdot \tau + S_M \quad (2)$$

$$\tau = \mu\left[\nabla V + [\nabla V]^T - \frac{2}{3}\delta \nabla \cdot V\right] \quad (3)$$

Where "τ" represents the generalized form of the Cauchy stress tensor for a Newtonian fluid. "ρ" denotes the density of the water in kg/m^3 matrix, "V" *is* the free-stream velocity (m /sec), and "δ" is the identity matrix.

In transient analysis, the turbine rotor is physically rotated at each time step using ANSYS CFX's transient rotor-stator scheme, which is based on the sliding-mesh technique. The transient rotor-stator approach models the relative motion between the External Domain (ED) and Internal Domain (IRD). The external domain remains stationary, while the internal domain rotates at an angular speed of 0.74 rad/sec. This approach provides a more realistic simulation of turbine rotation than the steady-state approach.

However, to achieve faster convergence, the steady-state solution obtained from the Multiple Frame of Reference (MFR) approach is used as the initial condition for the transient simulation. MFR-

based steady-state simulations use the frozen rotor technique, in which the relative positions of the two domains remain fixed, while the reference frame for the solution rotates. This approach has also been employed by other researchers [25].

For numerical accuracy, the high-resolution advection scheme is applied, and the second-order backward-Euler option is used in the transient scheme. The convergence criteria are set based on RMS residuals, with a specified value of $1 \times 10{-}4$.

The Computational Fluid Dynamics (CFD) model solves the Reynolds-Averaged Navier-Stokes (RANS) equations, employing the Shear Stress Transport (SST) turbulence model to close the RANS equations [26]. Additionally, an automatic wall function is applied to resolve the boundary layer efficiently at low computational cost.

The SST model is an eddy viscosity model that combines the Wilcox $k-\omega$ model and the standard $k-\epsilon$ model using a blending function [27]. It performs well in regions at the onset of flow separation and under adverse pressure gradients. Over the past decade, researchers have successfully applied the shear stress transport (SST) model for tidal current turbines (TCTs) [17]. Therefore, the SST model is adopted for all simulations in this study.

The numerical model used in this study has been previously validated against experimental data in earlier research [28].

2.1. Computational domain and boundary conditions

The computational domain is divided into two parts: the cylindrical Internal Rotating Domain (IRD)and the Rectangular External Stationary Domain (ESD). The External Domain consists of the IN, MID, and OUT sections. The Internal Cylindrical domain encloses the blades, part of the nacelle, and the hub of the turbine. Its diameter is 24 m, while its width is set to 5.4 m. The length, height, and width of the Rectangular External Domain are set at 500 m, 40 m, and 54 m, as shown in Figures 1 and 2. The turbine is positioned 100 m from the inlet of the Rectangular External Domain, with the center of the hub's back face located at (x, y, z) = (0, 0, 0). The turbine is located at mid depth of the domain, ensuring a 10 m clearance between the blade tips and both the top and bottom of the computational domain to minimize the effects of the free surface at these boundaries [29]. Additionally, the turbine is placed off the centerline of the ESD to provide a more realistic representation of the turbine's behavior and to utilize the symmetry boundary condition, which reduces computational cost. Because the real turbine consists of two rotors, but only one rotor is simulated in this study, a symmetry boundary condition is applied to approximate the effect of the second rotor. The velocity at the inlet is set to 1.5 m/s with 5% turbulence intensity, while the outlet boundary of the External Stationary Domain is set to a relative static pressure of 0 Pa [30, 31]. Boundary conditions are defined as follows [32]:

- A no-slip wall boundary condition is applied to the bottom wall and one side of the domain.
- A free-slip boundary condition is applied to the top boundary of the domain.
- A no-slip wall boundary condition is also applied to the blades, hub, nacelle, and tower, assuming zero velocity adjacent to the wall, which is the most common type of wall boundary condition

Three interfaces are defined at the faces shared by the cylindrical Internal Rotating Domain and the Rectangular External Domain. These interfaces facilitate data transfer between the rotating and stationary domains [33]. The details of the different parameters, boundary conditions, and their settings are tabulated in Table 2.

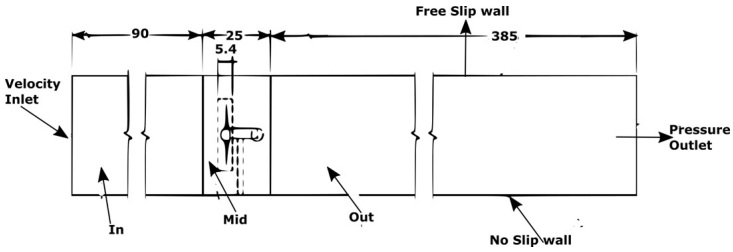

Figure 1. Demonstration of the computational domain

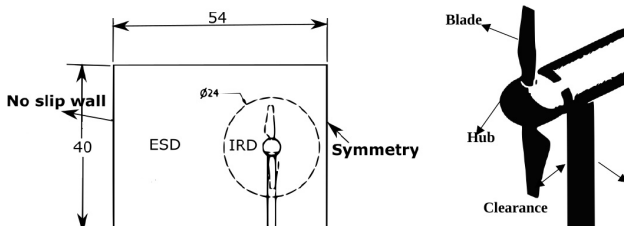

Figure 2. (a) Front view of computational domain **(b)** Turbine

2. 2. Mesh generation

A hybrid mesh and selective body meshing with patch-conforming meshing techniques are employed to discretize the entire computational domain [2, 5].

The meshing process begins with the turbine blades, followed by the hub, nacelle, tower, internal rotating domain (IRD), and external stationary domain (ESD). The patch-conforming method is applied to the turbine hub, nacelle, and tower. In this approach, all boundaries and faces conform within a small tolerance, ensuring a well-structured mesh. A conformal mesh is generated on the shared faces of the computational domain by geometrically modeling the rotor and IRD as a single part containing multiple bodies in ANSYS Design Modeler [34].

A Tetrahedral mesh is applied to the hub, nacelle, and tower, with element sizes set to 60 mm, 80 mm, and 100 mm, respectively. The surface of the blade is meshed using a structured meshing tech-

nique, with 190 divisions along the leading edge, 180 divisions along the trailing edge, and 90 divisions along the airfoil section at the tip. The IN and OUT portions of the Rectangular External Stationary Domain (ESD) are meshed using a structured mesh. The OUT portion comprises 194 divisions, while the IN portion comprises 45. The widths and heights of all three portions are identical and are divided into 40 and 30 divisions, respectively. The MID portion of the ESD is discretized using a tetrahedral mesh with an element size of 1000 mm, ensuring conformal meshes at the interfaces shared with the IRD and the ESD. The IRD is discretized using a tetrahedral mesh with an element size of 260 mm. A prism layer is applied to the turbine blades to accurately model flow behavior over the blade surfaces. The first-layer thickness inflation option is set with a first-layer height of 0.7 mm and a growth rate of 1.2. A maximum of 11 layers is specified, manifested in Figure 4 to maintain the prescribed range of 2 ≤ ≤ 300 as recommended by ANSYS CFX for proper automatic wall treatment in the SST turbulence model [35]. The IRD contains 3.1 million elements, accounting for approximately 73% of the total number of elements, whereas the ESD contains 1.1 million elements, as illustrated in Figure 3. The detail mesh metric is tabulated in Table 1.

Mesh refinement near the blades in the IRD is critical to ensure accurate near-wall treatment and precise prediction of flow separation over the blades [36, 37].

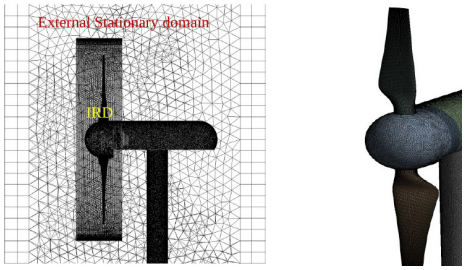

Figure 3. (a) Hybrid mesh of the complete domain **(b)** Mesh of the turbine

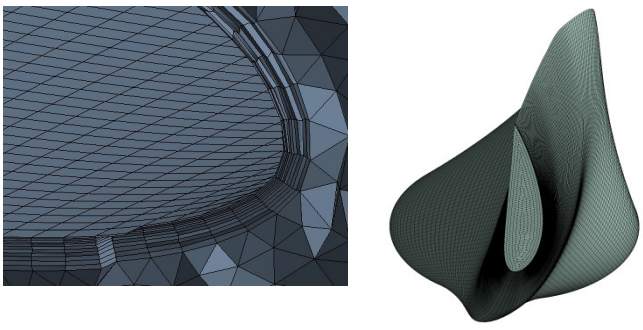

(a) **(b)**

Figure 4. (a) Boundaries layers on blades **(b)** Top view of turbine blade

Table 1. Mesh type in internal rotating domain and external stationary domain

Domain type	Mesh type	No of elements
Internal rotating domain (IRD)	Tetrahedral	3.1 mil
External stationary domain (ERD)	Hexahedral	1.1 mil
Total number of elements		4.2 mil

3. Performance parameters

In this section, three performance parameters of the tidal current turbine are discussed:

Where "R" is the radius of the rotor measured in meters, "ω" is the angular velocity of the rotor, expressed in radians/ second, whereas "V" is the velocity of the free stream velocity at hub height, measured in meter/second.

$$\text{Tip Speed Ratio (TSR)} = \frac{R\omega}{V_\infty} \quad (4)$$

Where "p" is the power available in the flow stream, "ρ" is the density of the water, and "A" is the swept area of the rotor. It is the main parameter used to evaluate the performance of the tidal current turbine. It represents the ratio of the power extracted by the turbine to the power available in the flow stream.

$$\text{Coefficient of performance } (C_P) = \frac{P}{0.5\rho A V_\infty^3} \quad (5)$$

$$\text{Coefficient of thrust } (C_t) = \frac{T}{0.5\rho A V_\infty^2} \quad (6)$$

Table 2. Parameters and its setting

Parameter	Setting
Analysis	Transient, total time- 85.6 sec, Time step-0.14 sec
Cylindrical domain	Non-buoyant, rotating, SST, wall function-automatic
Rotor	No-slip wall, rotating at 0.7 rad/sec, mesh Motion option-unspecified/system coupling, Mesh deformation- region of motion specified
Inlet	Subsonic, normal speed-1.5 m/sec, medium turbulence intensity-5%
Outlet	Subsonic, static pressure- 0 Pa
Side Wall	Symmetry
Bottom and one other side	No-slip wall
Top	Free-slip wall
Three interfaces	General connection, transient rotor stator, mesh connection-GGI
Convergence criteria	RMS residual 1x

4. Results and discussion

In this section, we investigate the impact of blade tip-to-tower clearance on the performance and stability of the St. Anthony Falls Laboratory (SAFL) Reference Model 1 (RM1) full-scale turbine, operating at a Tip Speed Ratio (TSR) of 4.87. In particular, the study investigates the effect of tip-to-tower clearance on turbine performance and the thrust force acting on the support structure, to improve understanding of the mechanisms underlying blade-tower interaction. Ten full-rotation time steps were performed for the turbine, corresponding to 90 s of physical time, with a time step of 0.1432 s. The initial layout of the turbine is presented in Figure 5.

The transient analysis was conducted for approximately 600-time steps, with each time step corresponding to the rotor's advancement through a discrete angular increment. For numerical convenience, the rotor is advanced by 6 degrees at each time step, which requires 60-time steps to cover a full 360° rotation. The parameters "C" and "d" stand for the clearance between the blade tip and the tower and the tower's diameter, respectively. The whole number following "C" and d" represents the length of the clearance and the diameter of the tower.

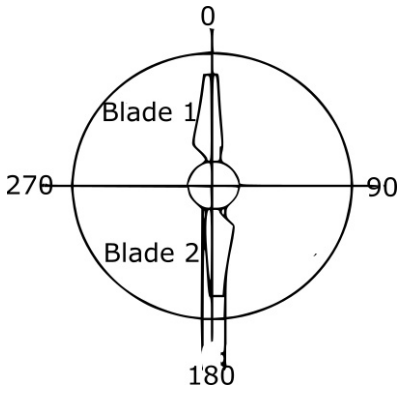

Figure 5. Initial condition of the turbine.

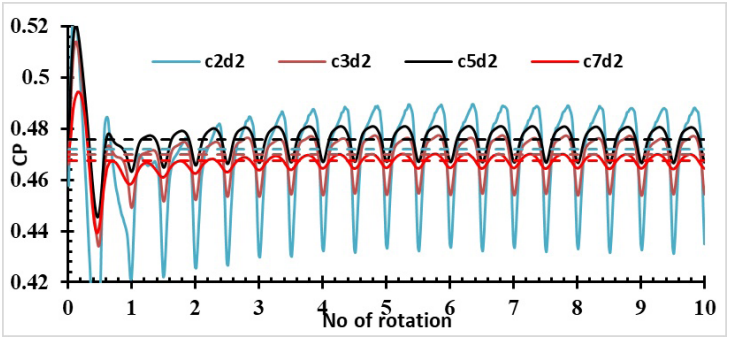

Figure 6. Coefficient of performance (C_p) for complete ten rotations

Figure 6 illustrates the C_p for a turbine with varying blade tip-to-tower clearances, while maintaining a constant tower diameter of 2 meters. The simulations span ten rotations, with a focus on the final rotation due to its relative stability.

It is evident that the tower significantly impacts both the coefficient of performance and thrust. Specifically, when a turbine blade aligns with the tower, the coefficient of performance is relatively low. The C_p increases smoothly as the blade rotates away from the tower and then begins to decrease again as the blade approaches the tower. These fluctuations are attributed to the tower shadow effect, which refers to the alteration of the local flow field due to the presence of the tower, resulting in localized decreases in flow velocity near the tower and thus temporarily reducing power extraction.

A detailed analysis of this phenomenon is required to enable optimal turbine design and positioning, particularly to avoid significant changes in performance due to flow patterns affected by the tower wake [38-40].

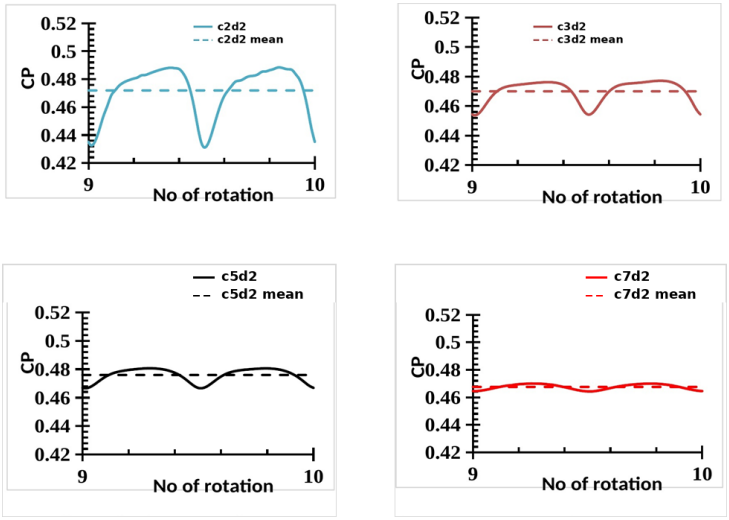

Figure 7. Coefficient of performance (C_p) for 2 m, 3 m, 5 m, & 7 m blade tip-to-tower clearance having 2 m diameter tower

As shown in Figure 7, variations in blade tip-to-tower clearance have a negligible influence on the mean C_p values. Specifically, clearances of 7 m and 5 m yield mean C_p values of 0.476 and 0.468, respectively, whereas clearances of 3 m and 2 m both yield a mean C_p of 0.472. The maximum deviation is 0.016, which corresponds to a relative change of approximately 1.69% compared to the reference value of 0.476.

However, given the inherent limitations of Reynolds-Averaged Navier–Stokes (RANS)-based Computational Fluid Dynamics (CFD) simulations, such small differences fall within the range of numerical uncertainty. As such, they cannot be conclusively attributed to variations in tip-to-tower clearance. Although RANS models are computationally efficient, they provide reduced accuracy in prediction of the effects of complex turbulent flow when considering separation and recirculation regions in the flow.

Therefore, the minor variations observed in the mean C_p are more likely attributable to numerical errors and model limitations as-

sociated with RANS-based simulations than to blade tip-to-tower clearance.

Table 3. Fluctuations of the performance coefficient (C_p) relative to its mean value

Blade tip-to-tower clearance (m)	Mean(C_p)	Fluctuation %
7	0.468	1.24
5	0.476	2.98
3	0.470	4.98
2	0.472	12.23

Fluctuation=(max-min)/ (mean C_p)

Variations in tip-to-tower clearance produce a significant effect, causing large variations in C_p about the mean, that increase in magnitude as the clearance decreases. This behavior is attributed to the increased blockage effect of the tower, pushing the rotor further into the area influenced by the tower shadow effect.

This trend is consistent with the observations published in a similar experimental study [41], which examined the effect of mast closeness on rotor loads. When the relative position of a dummy mast changes, the mean load remains constant, while the coefficient of variation (COV) increases, indicating greater load fluctuations.

Furthermore, it is noteworthy that the dependence of the reduction in clearance on the magnitude of fluctuation is nonlinear. As tip-to-tower clearance decreases to small values, the fluctuation increases sharply, as presented in Table 3.

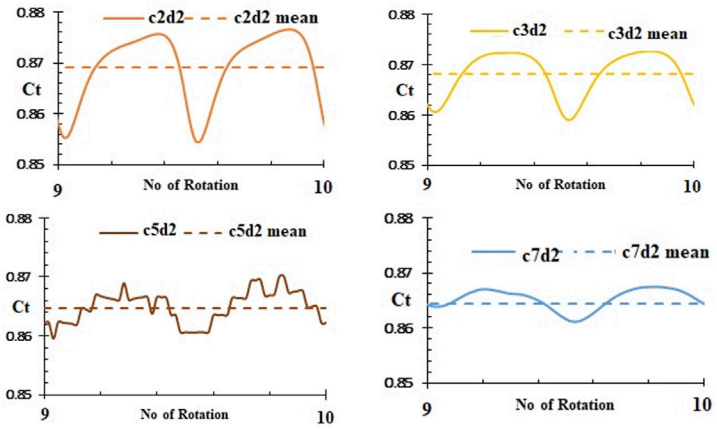

Figure 8. Coefficient of thrust (C_t) for blade tip-to-tower clearances of 2 m, 3 m, 5 m, and 7 m

Figure 8 illustrates the variation of the coefficient of thrust (C_t) for different blade tip-to-tower clearances. C_t exhibits a trend similar to that of C_p as the relative angle between the turbine blade and the tower varies. The thrust force on the blade is large when the blade is at positions away from the upstream region of the tower. Thus, C_t is higher at these positions. However, C_t decreases as the blade approaches the tower. This is consistent with results published in previous studies concerning different tower diameters [21].

While the mean coefficient of thrust does not appear sensitive to changes in blade tip-to-tower clearance, the deviation from the mean, used as a measure of performance stability, varies considerably. At a clearance of 2 m, the deviation from the mean is the largest, with a value of 8.45%, followed by 3 m, 5 m, and 7 m at 7.96%, 6.18%, and 5.98%, respectively, as presented in Table 4.

Table 4. Variation of the coefficient of thrust (C_t) relative to its mean value

Blade tip-to-tower clearance (m)	Mean (C_t)	Fluctuation %
2	0.86	8.45
3	0.86	7.96
5	0.87	6.18
7	0.87	5.98

These observations show that lower tip-to-tower clearances lead to increased fluctuations in hydrodynamic forces on the turbine blades and consequently, to increased thrust fluctuations. Such unsteady forces may have implications for the structural integrity and operational reliability of the turbine.

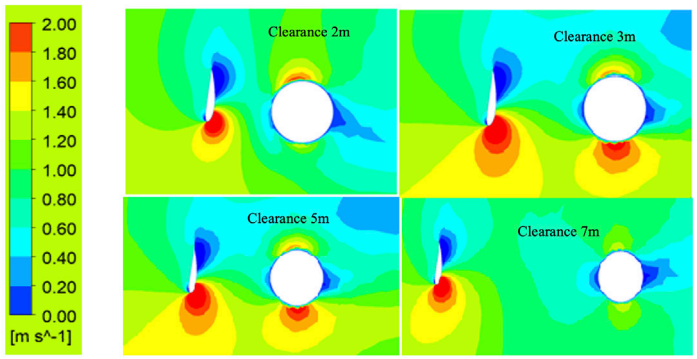

Figure 9. Velocity contour for different blade tips to tower clearance

Figure 9 presents the velocity contours at a radial distance of 7 m below the nacelle for varying tip-to-tower clearances. As expected, the velocities are observed to be significantly reduced upstream and downstream of the tower when compared to the overall flow field. The reduction in velocity around the tower is the so-called "tower shadow effect", the existence of which is evident through the low-velocity region (blue/green contours) upstream of the tower.

The flow along the blade, in all cases considered, displays the typical pattern of acceleration toward the trailing edge on the suction side

after initial acceleration near the leading edge. As discussed previously, the observed reduction in both the C_p and C_t is primarily associated with the blade's periodic entry into the tower-shadow region, as reflected in the velocity field.

The magnitude of the tower shadow effect increases as the tip-to-tower clearance decreases, whereas a larger tip-to-tower clearance corresponds to reduced interaction with the disturbed flow region around the tower. Thus, a larger tip-to-tower clearance would mitigate tower-induced flow disturbances, thereby decreasing unsteady loads and the risk of fatigue failure in the blades and supporting structure, especially under cyclic operating conditions.

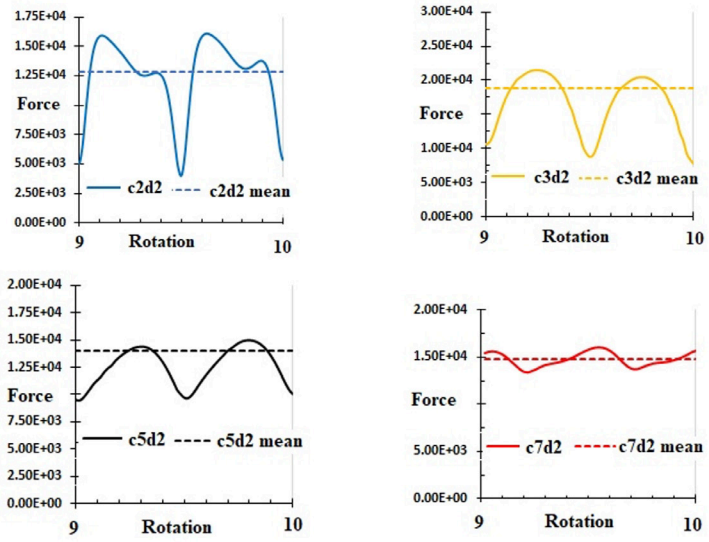

Figure 10. Thrust force (N) acting on the tower for blade tip-to-tower clearances of 7 m, 5 m, 3 m, and 2 m (Tower diameter = 2 m)

Figure 10 shows the evolution of the thrust force acting on the tower over time for various tip-to-tower clearances. When the blade is directly upstream of the tower, the thrust on the tower is minimal. As the blade moves away from the upstream position, the thrust magnitude increases with angular displacement, reaches a maximum, and then decreases. This behavior is attributed to modifications in the local flow field around the tower due to blade-tower interaction.

In addition, as the blade passes in front of the tower, the location of the stagnation point on the tower surface and the characteristics of flow separation are modified. Similar flow interference mechanisms have been reported in studies of wind turbines [42].

The magnitude and periodicity of the thrust force on the tower are also influenced by the blade tip-to-tower clearance. This effect is more pronounced at smaller tip clearances, producing higher *2P* oscillation amplitudes in the tower thrust force signal than at larger tip clearances, which is consistent with previous studies on tidal turbines.

Results indicate that the amplitude of thrust force fluctuations reaches approximately 98% of the mean when the tip-to-tower clearance is 2 m. With increasing tip-to-tower clearance, this fluctuation drops sharply to 18.7% at 7 m, as presented in Table 5.

Table 5. Fluctuations in the thrust force acting on the tower for different blade tip-to-tower clearances.

Tip-to-tower clearance (m)	Mean thrust force (N)	Fluctuation %
2	12800	97.9
3	18800	96.5
5	14000	67.4
7	14800	18.7

The magnitude and periodicity of the thrust force on the tower are also influenced by the blade tip-to-tower clearance. This effect is more pronounced at smaller tip clearances, thus producing higher 2P oscillation amplitude in the tower thrust force signal compared to larger tip clearances, which is consistent with findings reported in previous studies on tidal turbines.

The substantial reduction in fluctuation amplitude highlights the significance of tip-to-tower clearance in achieving smoother turbine loading conditions and, consequently, improved performance stability.

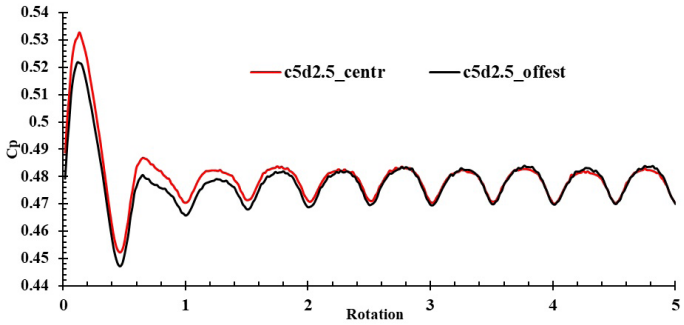

Figure 11. Coefficient of performance (C_p) with and without the symmetry boundary condition

Figure 11 shows the C_p of the turbine over five rotations under two different boundary-condition configurations. The first configuration employs symmetry boundary conditions, with the turbine placed asymmetrically within the computational domain; the second applies a no-slip wall boundary condition on one domain boundary, with the turbine positioned asymmetrically within the domain.

The above figures show that C_p does not vary significantly between the two configurations. During the 4th and 5th rotations, the variations were less than 5%. Thus, it may be concluded that the type of boundary condition used, i.e., symmetry or no-slip wall, has a negligible effect on the turbine performance predicted by the present simulations.

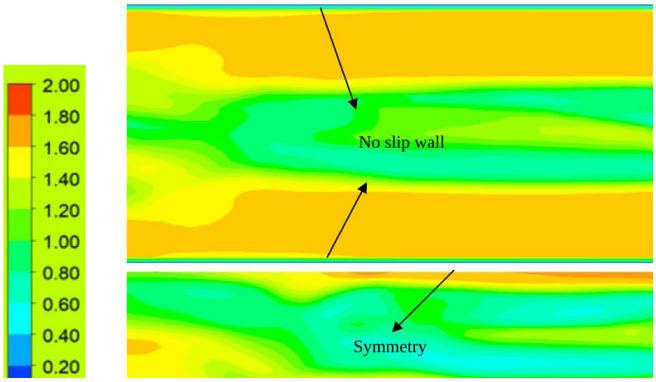

Figure 12. Velocity contours for symmetry and no-slip wall boundary conditions

Figure 12 further illustrates this observation by presenting velocity-contour fields for both configurations. A low-speed region downstream of the turbine is evident in both configurations (blue-green colors indicate low speed), whereas a region of increased velocity can be observed on either side of the turbine wake. The consistency of the flow fields between the two cases provides evidence that boundary-condition selection has a negligible influence on performance parameters and flow characteristics.

This result aligns with established Computational Fluid Dynamics (CFD) practices. At a symmetry boundary, the normal velocity component is zero, representing a mirrored flow condition, whereas a no-slip wall enforces zero velocity at the boundary due to viscous effects. In both cases, the velocity at the boundary is zero. However, since the performance remains largely unchanged between these conditions, it can be inferred that either boundary condition is suitable for this type of simulation.

5. Conclusion

In this study, the effect of the tip-to-tower clearance on the overall performance and aerodynamic characteristics of the wind turbine is investigated. Turbine performance is evaluated using the coefficient of performance (C_p) and coefficient of thrust (C_t). Blade-tower interaction at different tip clearances is studied by analyzing the thrust force acting on the tower. Numerical simulations are performed on the full-scale SAFL RM1 turbine for ten complete rotations, employing the Reynolds-Averaged Navier-Stokes (RANS) approach in ANSYS CFX to model various tip-to-tower clearances.

The results indicate that the mean C_p remains largely insensitive to variations in blade tip-to-tower clearance. Specifically, for clearances of 7 m and 5 m, the mean C_p values are 0.468 and 0.476, respectively, for clearances of 3 m and 2 m, the corresponding mean values are 0.472 and 0.470. However, the magnitude of fluctuations about the mean C_p increases significantly with decreasing blade tip-to-tower clearance. At a clearance of 2 m, the fluctuation in C_p is 12.23%; at clearances of 3 m, 5 m, and 7 m, it is 4.98%, 2.98%, and 1.23%, respectively.

A similar trend is observed for C_t. While the mean C_t remains relatively stable, approximately 0.87 for clearances of 7 m and 5 m, and approximately 0.86 for 3 m and 2 m, the magnitude of fluctuations increases as clearance decreases. Specifically, the fluctuation reaches 8.45% at a 2 m clearance, followed by 7.96%, 6.18%, and 5.98% for clearances of 3 m, 5 m, and 7 m, respectively. Notably, this increase in fluctuations is a nonlinear phenomenon that becomes more pronounced with decreasing clearance.

The variation in thrust on the tower with respect to blade tip-to-tower clearance is also significant. Changes in the location of stagnation point and altered flow separation patterns are observed as the blade passes across the tower, resulting in fluctuations in hydrodynamic loading on the tower structure. This fluctuation becomes highly pronounced at low clearances, with fluctuations around 98% relative to the mean at 2 m, compared with 96%, 67%, and 18% at clearances of 3 m, 5 m, and 7 m, respectively.

To summarize, tip-to-tower clearance has a negligible effect on the mean values of C_p and C_t, but is a major factor influencing the range of variation in performance parameters. Furthermore, the tower thrust varies substantially across different clearance settings, which could lead to increased fatigue loads on the blade and tower. As a result, tip-to-tower clearance must be carefully considered in the design of a tidal current turbine to manage unsteady loading and enhance structural reliability.

Finally, the simulations indicate that applying symmetry boundary conditions has minimal influence on turbine performance or wake. However, it provides clear advantages by reducing computational cost and is therefore an efficient approach for large-scale simulations.

Copyright and permission statement

All figures included in this manuscript are the authors' original work.

Nomenclature

SAFL	St. Anthony Falls Laboratory
RM1	Reference model 1
CFD	Computational Fluid Dynamic
S_M	Momentum source
μ	Dynamic viscosity
∇V	Velocity gradient
δ	Identity matrix
RANS	Reynolds-Averaged Navier-Stroke Equation

TSR	Tip speed ratio
SST	Shear stress transport
MRF	Multiple frames of reference
C_p	Coefficient of performance
C_t	Coefficient of thrust
T	Thrust force on the blade
P	Power available in water
R	Radius of the rotor
V_∞	Mainstream velocity (m/sec)
V	Vector of velocity V (x, y, z) (m/sec)
Ω	Angular velocity (rad/sec)
ESD	External stationary domain
IRD	Internal rotating domain
C2	Clearance 2 m
C3	Clearance 3 m
C5	Clearance 5 m
C7	Clearance 7 m
d2	Tower diameter 2m

References

[1] E. A. Lloyd, N. Oreskes, S. I. Seneviratne, and E. J. Larson, "Climate scientists set the bar of proof too high," Climatic Change, vol. 165, no. 3, p. 55, 2021.

[2] N. Kolekar and A. Banerjee, "Performance characterization and placement of a marine hydrokinetic turbine in a tidal channel under boundary proximity and blockage effects," Applied Energy, vol. 148, pp. 121-133, 2015.

[3] R. Jayabal, "Towards a carbon-free society: Innovations in green energy for a sustainable future," Results in Engineering, vol. 24, p. 103121, 2024.

[4] H. M. Zainal and O. K. Ahmed, "Effect of the design variables on the vortex water turbine performance," Journal of Thermal Engineering, vol. 11, no. 2, pp. 314-330, 2021.

[5] A. Gupta and L. Varshney, "Performance prediction for solar air heater having rectangular sectioned tapered rib roughness using CFD," Thermal Science and Engineering Progress, vol. 4, pp. 122-132, 2017.

[6] M. Ahmed Zaib et al., "Effect of Blade Diameter on the Performance of Horizontal-Axis Ocean Current Turbine," Energies, vol. 15, no. 15, p. 5323, 2022.

[7] M. Shamsuddin and N. M. Kamaruddin, "Experimental study on the characterization of the self-starting capability of a single and double-stage Savonius turbine," Results in Engineering, vol. 17, p. 100854, 2023.

[8] A. Al Naimat and D. Liang, "Substantial gains of renewable energy adoption and implementation in Maan, Jordan: A critical review," Results in Engineering, vol. 19, p. 101367, 2023.

[9] X. Liu et al., "A review of tidal current energy resource assessment in China," Renewable and Sustainable Energy Reviews, vol. 145, p. 111012, 2021.

[10] A. Farhoody and R. Shafaghat, "An experimental study to investigate the effect of pitch angle and wave characteristics on the performance of a horizontal axis tidal turbine," Applied Ocean Research, vol. 138, p. 103646, 2023.

[11] A. Roberts, B. Thomas, P. Sewell, Z. Khan, S. Balmain, and J. Gillman, "Current tidal power technologies and their suitability for applications in coastal and marine areas," Journal of Ocean Engineering and Marine Energy, vol. 2, no. 2, pp. 227-245, 2016.

[12] A. Røkke and R. Nilssen, "Marine Current Turbines and Generator preference. A technology review," 2013.

[13] P. Wang, L. Wang, Q. Zhang, F. Zhu, and B. Huang, "Performance and reliability study of China's first megawatt-scale horizontal-axis tidal turbine," Applied Ocean Research, vol. 138, p. 103648, 2023.

[14] S. Jan, S. Badshah, M. Badshah, and A. Javed, "Effect of tower elasticity on the performance and fatigue character of monopile support tower for tidal current turbine," Applied Ocean Research, vol. 106, p. 102446, 2021.

[15] N. Hafeez, S. Badshah, M. Badshah, and S. J. Khalil, "Effect of velocity shear on the performance and structural response of a small-scale horizontal axis tidal turbine," Marine Systems & Ocean Technology, vol. 14, no. 2, pp. 51-58, 2019.

[16] S. Hurubi, T. Stallard, H. Mullings, P. Stansby, and P. Ouro, "Numerical study of the effect of a ridge on the wake and loading of a tidal stream turbine," Journal of Fluids and Structures, vol. 129, p. 104158, 2024.

[17] M. Badshah, J. VanZwieten, S. Badshah, and S. Jan, "CFD study of blockage ratio and boundary proximity effects on the performance of a tidal turbine," IET Renewable Power Generation, vol. 13, no. 5, pp. 744-749, 2019.

[18] J. Liu, H. Lin, S. R. Purimitla, and M. D. ET, "The effects of blade twist and nacelle shape on the performance of horizontal axis tidal current turbines," Applied Ocean Research, vol. 64, pp. 58-69, 2017.

[19] M. Zormpa, "Actuator line modelling of wind turbines and their wakes," University of Oxford, 2024.

[20] A. Mason-Jones, D. M. O'Doherty, C. E. Morris, and T. O'Doherty, "Influence of a velocity profile & support structure on tidal stream turbine performance," Renewable energy, vol. 52, pp. 23-30, 2013.

[21] Z. U. Rehman, S. Badshah, A. F. Rafique, M. Badshah, S. Jan, and M. Amjad, "Effect of a support tower on the performance and wake of a tidal current turbine," Energies, vol. 14, no. 4, p. 1059, 2021.

[22] C. Hill, V. S. Neary, B. Gunawan, M. Guala, and F. Sotiropoulos, "US department of energy reference model program RM2: experimental results," Sandia National Lab.(SNL-NM),-Albuquerque, NM(United States);Univ. of …2014.

[23] M. M. Kamal, A. Abbas, T. Alam, N. K. Gupta, and R. Khargotra, "Hybrid cross-flow hydrokinetic turbine: Computational analysis for performance characteristics with helical Savonius blade angle of 135°," Results in Engineering, vol. 20, p. 101610, 2023.

[24] M. Badshah, S. Badshah, and S. Jan, "Comparison of computational fluid dynamics and fluid structure interaction models for the performance prediction of tidal current turbines," Journal of Ocean Engineering and Science, vol. 5, no. 2, pp. 164-172, 2020.

[25] H. Gao, W. Zhu, Y. Liu, and Y. Yan, "Effect of various winglets on the performance of marine propeller," Applied Ocean Research, vol. 86, pp. 246-256, 2019.

[26] J. Guerra, L. Velásquez, A. Rubio-Clemente, L. Jaramillo, and E. Chica, "Design and optimization of a siphon turbine using the response surface methodology," Results in Engineering, vol. 22, p. 102241, 2024.

[27] D. Cherrared, "Numerical simulation of film cooling a turbine blade through a row of holes," Journal of Thermal Engineering, vol. 3, no. 2, pp. 1110-1120, 2017.

[28] M. Badshah, S. Badshah, J. VanZwieten, S. Jan, M. Amir, and S. A. Malik, "Coupled fluid-structure interaction modelling of loads variation and fatigue life of a full-scale tidal turbine under the effect of velocity profile," Energies, vol. 12, no. 11, p. 2217, 2019.

[29] C.-H. Jo, D.-Y. Kim, Y.-H. Rho, K.-H. Lee, and C. Johnstone, "FSI analysis of deformation along offshore pile structure for tidal current power," Renewable energy, vol. 54, pp. 248-252, 2013.

[30] M. Badshah, S. Badshah, and K. Kadir, "Fluid structure interaction modelling of tidal turbine performance and structural loads in a velocity shear environment," Energies, vol. 11, no. 7, p. 1837, 2018.

[31] K.-P. Kim, M. R. Ahmed, and Y.-H. Lee, "Efficiency improvement of a tidal current turbine utilizing a larger area of channel," Renewable Energy, vol. 48, pp. 557-564, 2012.

[32] S. Badshah, M. Badshah, N. Hafeez, S. Jan, and Z. U. Rehman, "Cfd analysis of tidal current turbine performance with different boundary conditions," in IOP Conference Series: Earth and Environmental Science, 2020, vol. 581, no. 1, p. 012010: IOP Publishing.

[33] I. Ansys, "ANSYS meshing user's guide," vol, vol. 15317, pp. 724-746, 2013.

[34] C. Ansys, "Ansys CFX-solver modeling guide," Release, vol. 15, pp. 162-168, 2009.

[35] L. Rodríguez, A. Benavides-Moran, and S. Laín, "Three-bladed horizontal axis water turbine simulations with free surface effects," International Journal of Applied Mechanics and Engineering, vol. 26, no. 3, pp. 187-197, 2021.

[36] S. Salunkhe et al., "Validation of tidal stream turbine wake predictions and analysis of wake recovery mechanism," Journal of Marine Science and Engineering, vol. 7, no. 10, p. 362, 2019.

[37] A. C. Creech, A. G. Borthwick, and D. Ingram, "Effects of support structures in an LES actuator line model of a tidal turbine with contra-rotating rotors," Energies, vol. 10, no. 5, p. 726, 2017.

[38] G. Shoukat, B. Gaurier, J.-V. Facq, and G. Payne, "Experimental investigation of the influence of mast proximity on rotor loads for horizontal axis tidal turbines," Renewable Energy, vol. 200, pp. 983-995, 2022.

[39] A. C. Creech, A. G. Borthwick, and D. J. E. Ingram, "Effects of support structures in an LES actuator line model of a tidal turbine with contra-rotating rotors," vol. 10, no. 5, p. 726, 2017.

[40] C. J. R. Ansys, "ANSYS CFX solver modeling guide," vol. 15, pp. 162-168, 2009.

[41] G. Shoukat, B. Gaurier, J.-V. Facq, and G. J. R. E. Payne, "Experimental investigation of the influence of mast proximity on rotor loads for horizontal axis tidal turbines," vol. 200, pp. 983-995, 2022.

[42] Y. Shkara, R. Schelenz, and G. Jacobs, "The effect of blade-tower interaction on the structure loading of multi megawatt horizontal axis wind turbine," in Journal of Physics: Conference Series, 2018, vol. 1037, no. 7, p. 072033: IOP Publishing.